Decoupled electron-phonon transport in Ag_2Se thermoelectric materials through constructing TiO_2/MoS_2 co-decorated cell-membrane-mimic grain boundaries

Hanwen Hu[a], Yiyan Liao[b], Shanshan Tan[b], Chen Li[a], Jun Tang[c], Kun Zheng[a,*], Lei Yang[b,*]

[a]Beijing Key Laboratory of Microstructure and Properties of Solids, Beijing University of Technology, Beijing 100124, China.

[b]School of Materials Science & Engineering, Sichuan University, Chengdu, 610064, China.

[c]Key Laboratory of Radiation Physics and Technology, Ministry of Education, Institute of Nuclear Science and Technology, Sichuan University, Chengdu 610064, China.

[*] **Corresponding authors**

*E-mail: lyang1986@scu.edu.cn (L. Yang); kunzheng@bjut.edu.cn (K. Zheng).

Fig. S1.

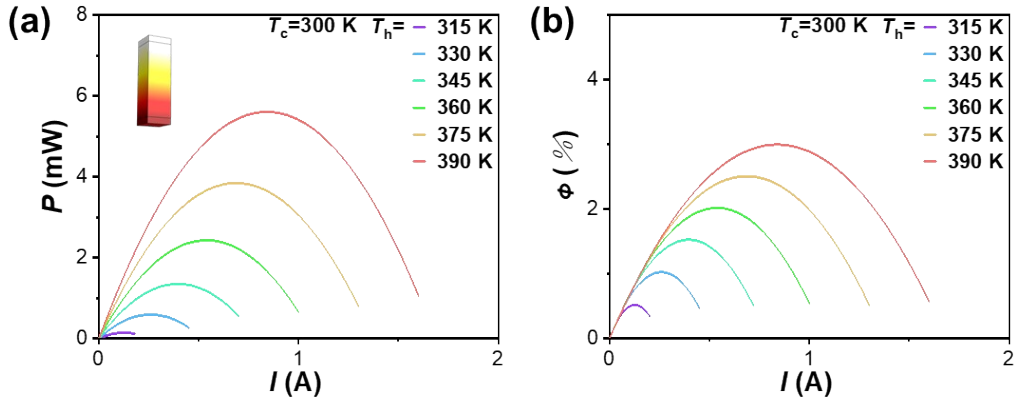

Fig. S1. (a-b) The results of the finite-element analysis of the Ag_2Se based module detail the output power (P) and conversion efficiency (Φ) of the Ag_2Se based module as a function of current (I) with a fixed cold side temperature (T_c) and varied hot side temperature (T_h).

Fig. S2.

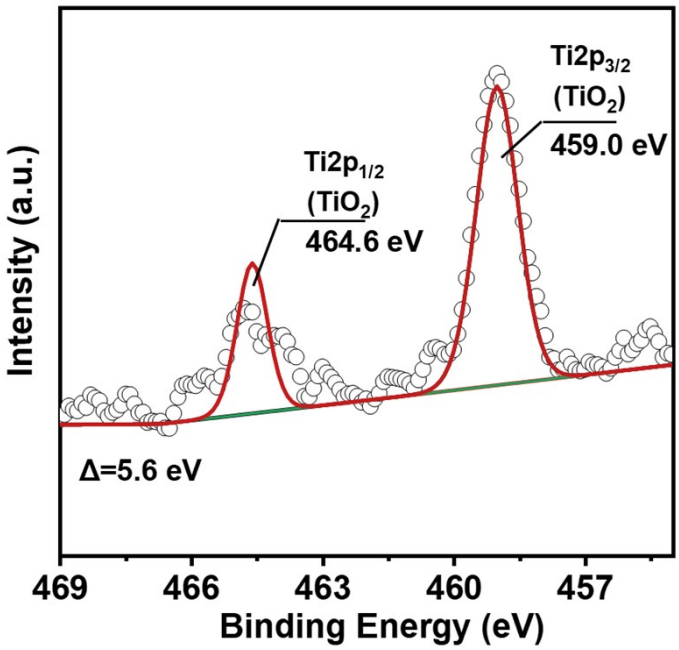

Fig. S2. High resolution XPS spectra of the AS-T-0.5 MoS_2 powder sample, inset is the Ti 2p spectrum.

Fig. S3.

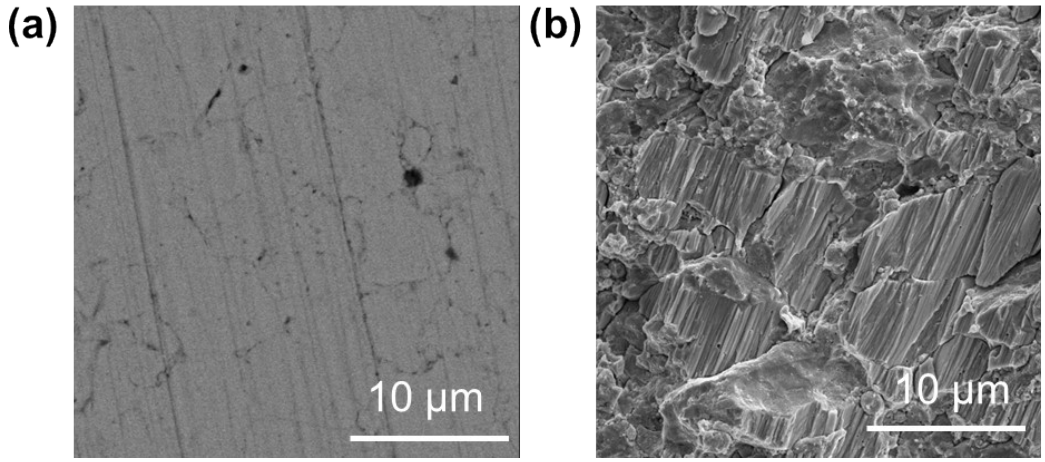

Fig. S3. (a) As-synthesized Ag_2Se to the as-decorated bulk samples. (b) The cross-section SEM of Ag_2Se bulk samples.

Fig. S4.

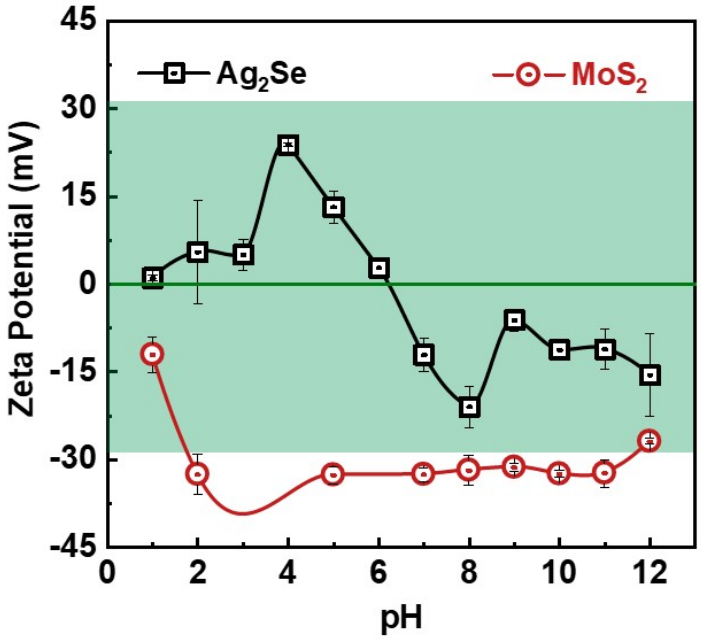

Fig. S4. Zeta potential of MoS_2 and Ag_2Se dispersion at different pH.

Fig. S5.

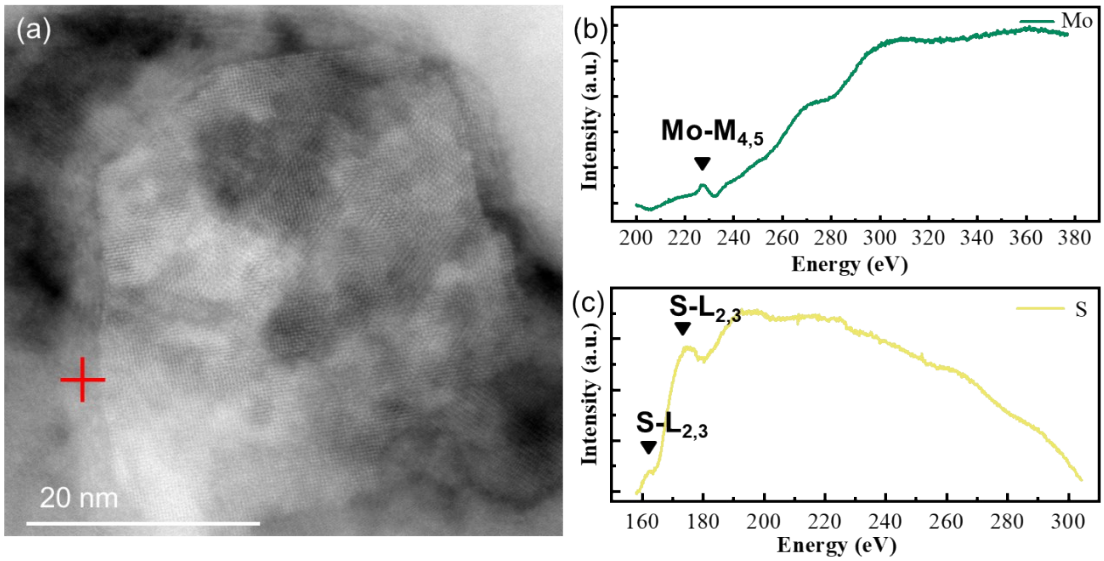

Fig. S5. (a) STEM-HAADF image of the TiO_2/MoS_2 co-doped Ag_2Se nanocomposites (b-c) EELS spectra of the element of Mo and S collected from a MoS_2 area (red cross).

Fig. S6.

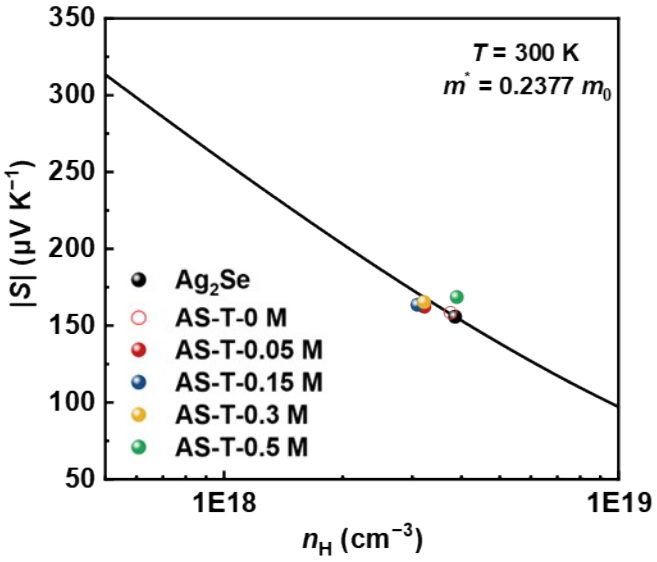

Fig. S6. The variation of S with n_H carrier concentration for of AS-T-*x* M (where *x* = 0, 0.05, 0.15, 0.3, and 0.5 in wt%) compared to the Pisarenko line, which is caused by the change in the increased effective density of states mass (*m**).

Fig. S7.

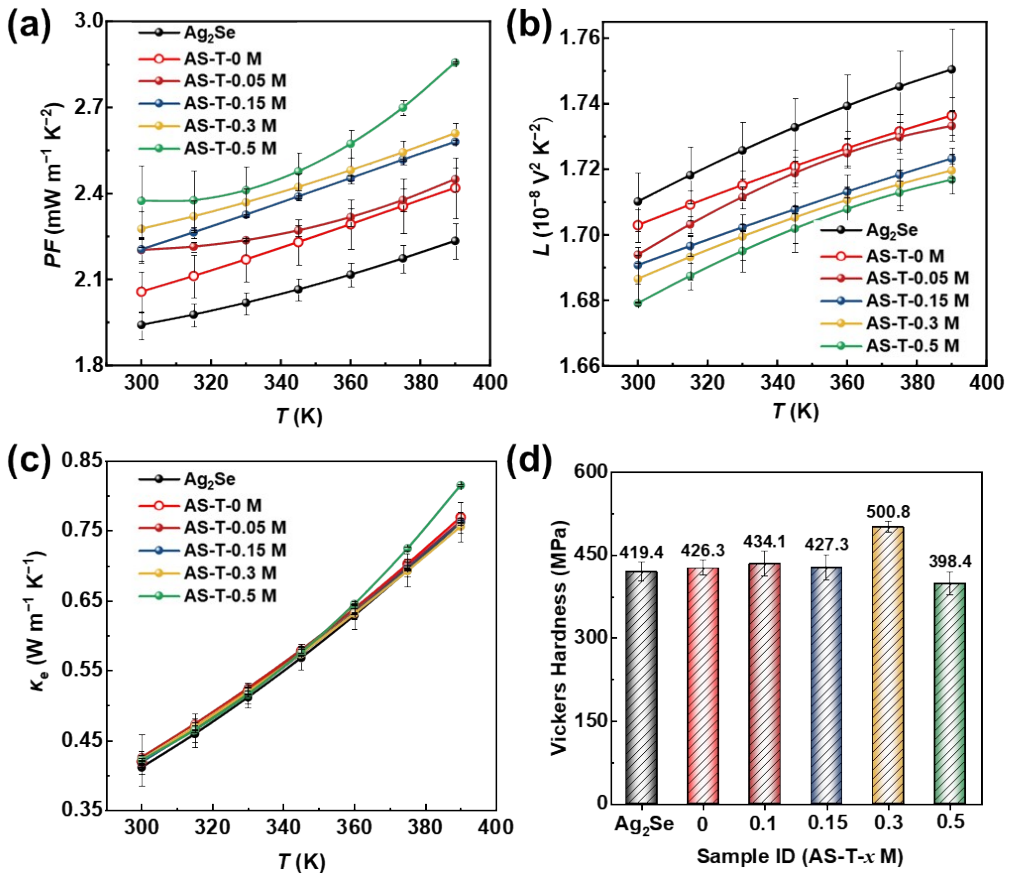

Fig. S7. Temperature-dependent (a) power factor (*PF*), (b) lorentz number (*L*), (c) electrons thermal conductivity (κ_e) and (d) the Vickers hardness (*Hv*) of AS-T-*x* M (where *x* = 0, 0.05, 0.15, 0.3, and 0.5 in wt%).

Fig. S8.

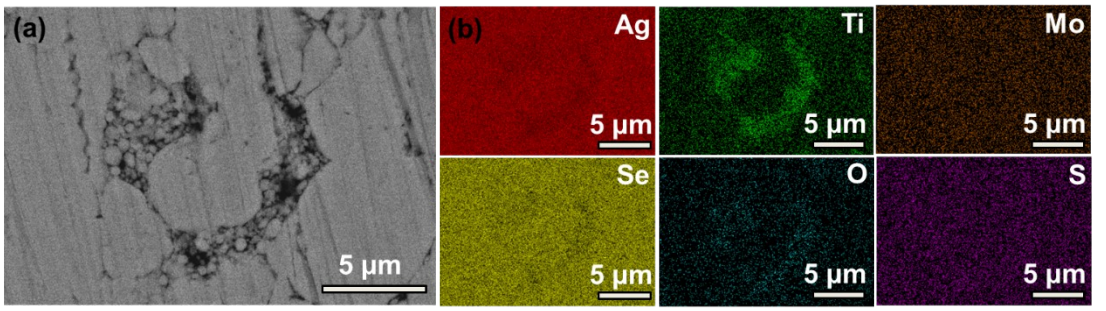

Fig. S8. (a)Low magnification SEM image of AS-T-0.5M sample. (b) Corresponding elemental distribution of Se, Ag, O, Ti, S, and Mo.

Table.S1

PH	1	2	5	7	8	9	10	11	12
Zeta Potential (mV)	-12.033	-32.566	-32.666	-32.566	31.833	31.333	32.466	32.333	-26.9
Error range	-3.0666	-3.4333	-1.5333	-1.1333	2.5333	-0.7666	-0.5666	-2.3666	0.5

Table.S2

Sample	Actual density	Relative density (%)
Ag_2Se	8.137	98.15
AS-T-0.05 M	8.020	96.74
AS-T-0.15 M	8.026	96.82
AS-T-0.3 M	8.007	96.59
AS-T-0.5 M	8.110	97.83